Icarus **156**, 373–386 (2002)
doi:10.1006/icar.2001.6794, available online at http://www.idealibrary.com on IDEAL®

Metastability of Liquid Water on Mars

Michael H. Hecht

Jet Propulsion Laboratory, M/S 233-200, 4800 Oak Grove Drive, Pasadena, California 91109
E-mail: michael.h.hecht@jpl.nasa.gov

Received May 30, 2001; revised October 19, 2001

A simple model of local heat transport on Mars demonstrates that transient melting of ice may occur in depressions and gullies nearly anywhere on the planet where thin ice is illuminated by normal-incidence insolation. An experiment has been performed to confirm the model of evaporation rate at low pressure. Reduction of radiative cooling due to gully geometry is shown to be important. Since appropriate meteorological, topographic, and optical conditions may occur on slopes nearly *anywhere* on the planet, hydrological features such as gullies would likely form only where such ice might accumulate, notably in sheltered locations at high latitudes. It is suggested that cold-trapping of winter condensation could concentrate a sufficient amount of ice to allow seasonal melting in gullies.

Key Words: **Mars; surface; ices; exobiology.**

INTRODUCTION

Recent pictures from the Mars Global Surveyor reveal features that appear to be young flow channels, claimed to be less than 1-myr old by Malin & Edgett (2000). While the topography of the features are consistent with the flow of liquid water, Malin and Edgett's suggestion that such a flow must be of catastrophic origin (e.g., bursting of an ice dam) has not been challenged. In fact, even though meteorological conditions on Mars have been understood for at least 25 years (e.g., Zurek 1992), it remains unclear whether water can flow on contemporary Mars. Atmospheric pressures on Mars straddle the triple point of water, while temperatures regularly cross the frostpoint. Unlike on Earth, atmospheric temperature has little influence on transient melting, since evaporative cooling of water dominates over convective exchange with the atmosphere. Not only is atmospheric convection negligible, but martian regolith is also highly insulating (Kieffer and Zent 1992). Consequently, large thermal gradients may exist as a result of local topography. Water in the liquid state might, in fact, exist under clement meteorological and favorable topographic contemporary conditions. It has been shown, for example, that martian ice can melt under favorable conditions such as in dusty snow (Clow 1987) or under a thick dust layer (Farmer 1976). In this work, similar thermal models are applied to martian gullies.

It has long been established (Carr 1983, McKay and Davis 1991) that liquid water, if present on Mars, could flow over extensive distances and persist for long periods of time. On Mars, as on Earth, water is ordinarily *meta*stable, evaporating or freezing slowly compared to the rate at which it flows across the surface. It will be shown here that while water on Mars would lose heat more rapidly from evaporative and radiative cooling and less rapidly from convective cooling than comparably cold places on Earth, the net difference is small. There is no intrinsic reason that, under the proper conditions, ice could not melt and flow in contemporary times if sufficient heat were present.

The preferential locations of the gully features at middle and high latitudes and altitudes, on pole-facing slopes, strongly suggests an association with cold traps that might harbor near-surface ice or condensate ice from nearby sources of water vapor. The most straightforward explanation of these gullies is seasonal melting. Moreover, since the features are only hundreds of meters in length, seasonal liquid water might only need to be present for hours at a time to carve them. This process might take the form of an actual trickle of water, even if such flow were as slow as 1 cm/s. It might also take the form of seasonal wetting of soil, causing preferential erosion or deflation. In the latter case, each gully might begin from condensation in an alcove, attaining its full length after years of downslope extension.

This paper reviews plausible conditions on Mars that would allow ice to melt. Older analyses (e.g., Wallace and Sagan 1979, Carr 1983, Kahn 1985, 1990, Goldspiel and Squyres 2000) modeled globally averaged or typical regional conditions to explain large-scale features but did not seek optimal combinations of atmospheric conditions and surface geometry that might produce local melting. More recently, Haberle *et al*. (2001) and Mellon and Phillips (2001) reexamined the stability of surface liquid water in disequilibrium on Mars, with both works affirming the general possibility of melting but arguing against liquid water at high latitudes. Neither of those works considered the influence of geometry or optical properties specific to gullies, as will be done here.

SURFACE–ATMOSPHERE EQUILIBRIUM

At the lower elevations found in much of the northern hemisphere of Mars, the present-day atmospheric pressure varies

0019-1035/02 $35.00

between 7 and 10 mbar. This pressure range is slightly, but distinctly, above the thermodynamic triple point of water, 6.1 mbar (4.6 Torr). Viking Lander 1, at 22°N latitude, measured 6.8–9.0 mbar, while Viking Lander 2, at 48°N latitude, measured 7.5–10 mbar. Mars Pathfinder, at 19.13°N latitude, measured the lowest values, 6.7–7.1 mbar (Haberle *et al*. 1999).

The low atmospheric pressure implies that the boiling point of pure water on much of Mars is 2–7°C above the melting point (and considerably higher for brackish water). By contrast, pure water on Earth exists over a 100°C temperature range at sea level. But the difference in stability of the liquid phase is far less than might be suggested by the difference in boiling point. On Earth, to raise the temperature from the melting point to the boiling point requires only 418.4 J/g, compared to 334 J/g to convert ice to water, and a full 2500 J/g to convert water to vapor (e.g., Berry *et al*. 1980). Furthermore, while the evaporation rate of water does increase with decreasing atmospheric pressure, it is even more strongly a function of temperature. Thus, at 0°C on Mars, water will evaporate no faster than 60°C water on Earth (see Eq. (15)). Freezing rates on Mars are limited by the rate that heat can be removed from an icy surface. Typical heat-loss processes, as will be seen, remove hundreds of watts per meter squared, compared to the $\sim$1 kW/m^2 latent heat required to freeze 1 cm/h. Water, therefore, can be expected to refreeze at rates not in excess of a few millimeters per hour. Consequently, neither evaporation nor freezing is an obstacle to the action of liquid water, even if such water were only a few centimeters deep.

At higher elevations, and hence over much of the southern hemisphere, Mars's atmospheric pressure is less than the triple point pressure of pure water. For water to be stable at this pressure, the surface temperature of the ice–water system must be a few degrees below the nominal melting point. Otherwise, the vapor pressure at the surface would exceed the ambient pressure, and the evaporating vapor would expand (and therefore cool) explosively. Unless some mechanism such as salinity reduces the melting point (and hence the vapor pressure), this requirement will force the formation of an ice crust as a thermal barrier between the liquid and the atmosphere. The actual thickness will be determined by the heat loss from the surface (typically no more than a few hundred watts per centimeter squared), the magnitude of the temperature drop, and the conductivity of the ice. Such a barrier would typically be a few millimeters or centimeters thick, and its presence would not substantially alter the argument presented here. For example, assuming the thermal conductivity of the ice is 0.022 W/cm $\cdot$ K, a 5°C temperature drop and 300 W/m^2 heat flow correspond to 3.67 cm of ice.

THERMAL EQUILIBRIUM

Ice will melt on Mars when the heat input from the Sun at the melting temperature exceeds the sum of the heat-loss processes from the ice. Comparison with cold climates on Earth is both instructive and deceptive. On Earth, convective losses to the atmosphere typically determine the thermal equilibrium between water and atmosphere. In the rarified air of Mars, convective losses are small since fewer molecules contribute to heat transfer. Conversely, evaporative losses are higher because of the longer mean free path of diffusing water molecules. Radiative losses to Mars's cold sky are somewhat greater than on Earth since, on Earth, the sky temperature is not significantly below the freezing point of water. Finally, conductive loss below the water is substantial if the bed consists of ice but is more modest for a bed of highly insulating martian soil (Kieffer and Zent 1992).

While evaporative cooling plays a major role in heat balance, the actual loss of water associated with evaporation may be ignored. If no heat sources are present, evaporation of 1 g of water will provoke freezing of 7.5 g, with the ratio determined by the respective latent heats. Despite vigorous evaporation (or, more accurately, as a result of such evaporation), a pool of water on Mars would first freeze, then slowly sublimate.

In this analysis, only direct insolation is considered as a source of heat. Scattering from the atmosphere is not considered because the assumption of optimal conditions implies that nearly the entire solar constant is directly absorbed by sun-facing surfaces on clear days. Long-wavelength radiation from the atmosphere is ignored because the air is assumed to be substantially colder than the surface temperature under optimal conditions. Exotic sources of heat, such as geothermal or chemical energy, are neglected.

The heat-loss processes considered are restricted to convective cooling to the atmosphere (assumed to be at a nominal temperature of 200 K), evaporative cooling, radiative cooling to an extremely cold sky, and conductive cooling to the ground. Less significant mechanisms, such as frictional cooling resulting from downhill flow, are neglected for simplicity. Also, no attempt is made to model the detailed vertical profile of absorption and heat loss in the ice–water–soil structure. Finally, thermal losses associated with transmission of solar radiation through thin capping ice (millimeters to a few centimeters thick) are ignored. It is assumed that any capping ice is reasonably transparent to radiation and that a significant portion of the heat intercepted by the ice will be conductively transported to the water. Carr (1983), for example, assumes an extinction coefficient between 0.006 and 1.0 cm^{-1}.

Figure 1 shows the thermal balance in histogrammic form for a pool of water, at the freezing point, under nominal martian conditions. The scenario depicted might be typical of published models (e.g., Wallace and Sagan 1979, Carr 1983, Kahn 1985, 1990, Goldspiel and Squyres 2000). It assumes conductive losses through a thick bed of ice (equilibrated for 1 h), and radiation from a high-emissivity, flat surface. Insolation, however, is assumed to be absorbed in a thin layer at the top of the ice (due, for example, to a dusty surface). Evaporation is calculated for open water under a 10-mbar atmosphere with little wind, but results would be similar for ice-encrusted water at lower pressures. The surface albedo is assumed to be 0.25, while actual values range from less than 0.1 to greater than 0.35 (see, for example, Mellon *et al*. 2000). The optical depth is 0.1,

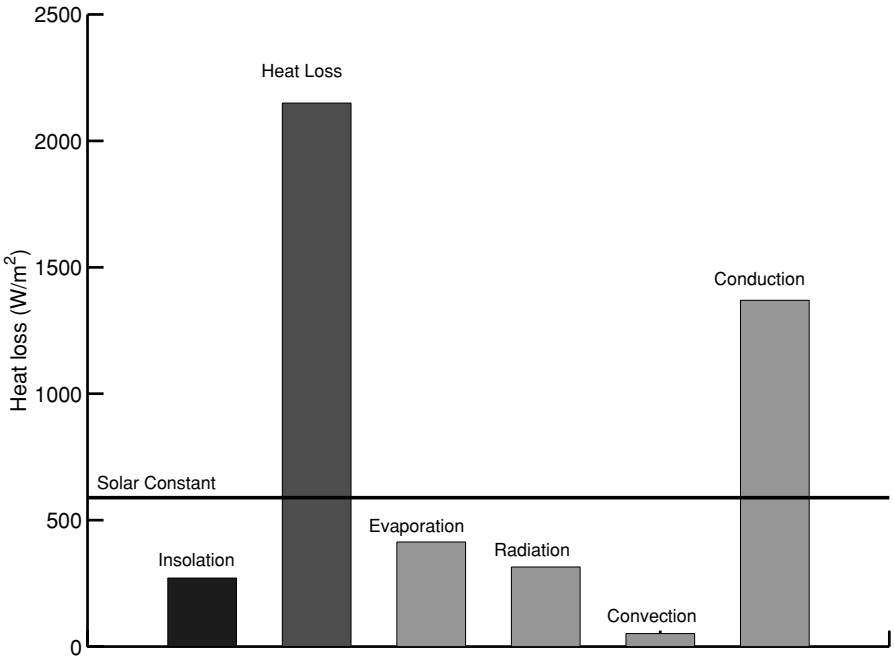

FIG. 1. Heat loss from water or ice at 273 K on Mars, compared to solar constant. The bar labeled "Heat Loss" is the sum of evaporative, radiative, convective, and conductive losses. Under these typical conditions, ice would not melt. See Table I for parameters and assumptions.

representing a clear sky (see Wolff *et al*. 1999, Leovy 2001, Smith *et al*. 2001), and the Sun angle is assumed to be 45° to the surface normal. The latter approximation is appropriate for phenomena requiring heat input over many hours, during which time the Sun moves across the sky, or for geometric averages over large areas.

For ice to melt, the total heat loss from the pool of water must be less than the heat input. For the conditions assumed in Fig. 1 it can be seen that evaporative losses, radiative losses, or conductive losses can each independently overwhelm the direct heat input from the Sun. Ice will not melt under these conditions. Despite the cold atmosphere, however, convective cooling is negligible. It follows that atmospheric temperature is a largely irrelevant measure of the "coldness" of Mars in this context. Poor convection also suggests that large thermal gradients might exist across the surface as a result, for example, of a transition from sunlit to shaded. Such gradients encourage the search for local surface conditions that might be anomalously warm.

The thermal balance in Fig. 2, in contrast, reflects more optimal, transient meteorological and geometrical circumstances (see Table I). It indicates a net gain in heat, resulting in a substantial rate of melting (approximately 1 mm/h). The calculation assumes low wind speeds (<2 m/s) and a clear atmosphere. It is restricted to times of day when incident sunlight is normal to local slopes. The Sun is only 10° above the horizon, over the pole at the southern summer solstice, near perihelion. The albedo is assumed to be 0.1, at the more extreme end of the measured distribution but consistent with high latitudes and the dark-colored gullies observed in the images. The local geometry is assumed to provide partial "shade" from the cold sky (i.e., low apparent emissivity). It is assumed that a thin sheet of ice overlays the soil (equilibrated for 2 h), because a thick ice sheet is too thermally conductive to support a sufficient thermal gradient at the surface. The calculation also assumes a surface temperature of −5°C. This lowering relative to the melting temperature may be due to the presence of 4–5 cm of ice on the water, 2–3 mol/liter

TABLE I
Physical Parameters Assumed for Figs. 1 and 2

Parameter	Fig. 1	Fig. 2
Solar constant (W/m^2)	589	701[a]
Albedo	0.25	0.1
Optical depth	0.1	0.1
Latitude	70°	75°
Sun zenith angle	45°	80°
Solar angle to local surface	45°	0°
Wind speed (m/s)	10	<2
Atmospheric pressure (mbar)	10	10
Atmospheric temperature (K)	200	200
Surface temperature (K)	273	267.4
Emissivity	1.0	1.0
Apparent emissivity	1.0	0.11[b]
Sky temperature (K)	100	100
Temperature of base (K)	200	223
Conductivity of base (W/cm · K)	0.022 (ice)	0.00077
Heat capacity of base (J/g · K)	2.01 (ice)	0.59
Density of base (g/cm^3)	0.9 (ice)	1.5
Equilibration time (h)	1	2

[a] At $L_S = 270$.
[b] At center of a depression with height (h) = diameter (d).

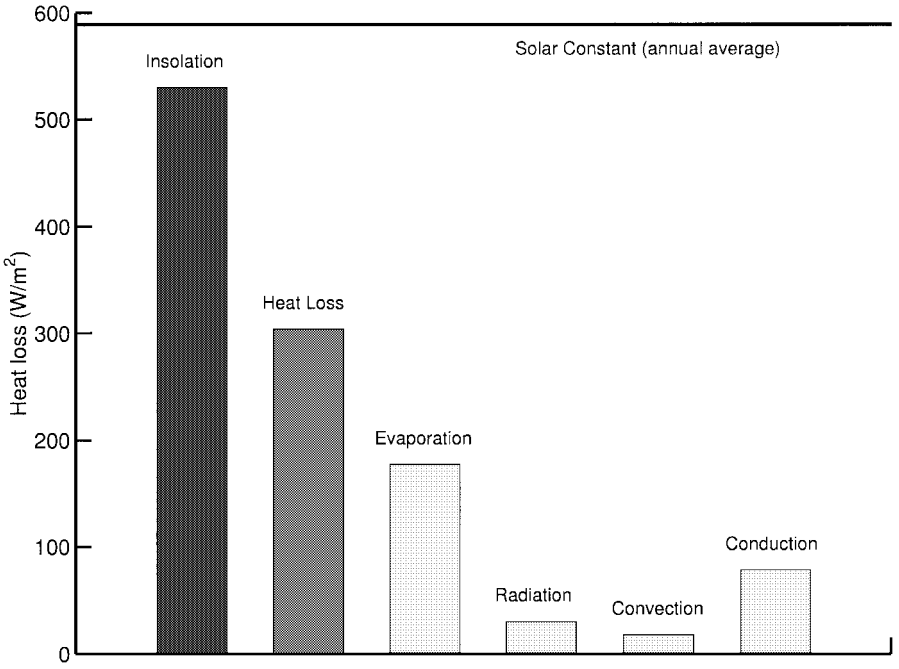

FIG. 2. Best-case heat balance, indicating in excess of 200 W/m^2 available for melting (corresponding to melt rate of 2 mm/h).

of dissolved salts in the meltwater, supercooling, or some combination of the three. An equivalent suppression of evaporation could result from dust or snow impeding the diffusion of vapor (Clow 1987, Farmer 1976).

EXPERIMENTAL OBSERVATION

To better understand the qualitative behavior of water at martian pressure, experiments were performed in a vacuum chamber equipped with an oil-free pump, dry nitrogen purge, and good illumination and visibility. A 3-in.-diameter stainless-steel dewar was filled with cold deionized water and placed in a vacuum chamber. The surface of the water was monitored with a commercial camcorder from outside the chamber, and the humidity was monitored with a General Eastern dewpoint hygrometer. The hygrometer head rested on a massive aluminum heat sink and was equipped with a small fan to draw gas past the mirror. Several methods were used to maintain the temperature of the liquid surface at or near 0°C, a requirement to prevent boiling. The most successful involved filling the vessel with weighted ice cubes, although this had the disadvantage of introducing modest amounts of dissolved gases into the water.

Since the evaporation rate depends on the difference between the surface vapor pressure and the ambient partial pressure of water, it is important that the air remain dry. For this reason a large cylindrical chamber with a radius of 15 in. and a horizontal length of 36 in. was chosen (0.42 m^3 volume). At the highest expected evaporation rate from the dewar, ~0.1 g/cm$^2 \cdot$ h, it would take approximately 30 min to raise the dewpoint to 0°C, corresponding to a density of 4.9 g/m^3 of water vapor. The dewpoint during the experiment was typically between −10 and −25°C, with values as high as −5°C reached at the lowest measured pressures. The effect of the background water vapor was numerically compensated in determination of the evaporation rate (see below).

The chamber served as a good analog for Mars with respect to the atmospheric pressure, but not the thermal environment. Both the surrounding gas and the walls were maintained at room temperature. Nitrogen gas was used rather than CO_2 since the ratio of buoyancy to viscosity forces ($R = g/v^2 = \rho^2 g/\mu^2$; see Table II) for nitrogen under Earth gravity is a better match to carbon dioxide under martian gravity at comparable pressure and temperature. Specifically, $R_{\text{Mars}}/R_{\text{Earth}} = 0.38$ for CO_2 and 1.33 for nitrogen, a comparison relevant to thermal convection. For mass convection (evaporation) it is more appropriate to compare $R' = \rho(\rho - \rho_w)g/\mu^2$. If ρ_w is taken as the saturation vapor pressure of water at the freezing point, 6.1 mbar, and the total atmospheric pressure ρ is taken as 10 mbar, then $R_{\text{Mars}}/R_{\text{Earth}} = 0.38$ for CO_2 and 2.2 for N_2.

Each experiment was initiated by purging the chamber with nitrogen, closing the nitrogen inlet, and then pumping the chamber to the target pressure as determined with a Granville–Phillips Convectron gauge. This step typically took several minutes to complete. The chamber dewpoint dropped precipitously during active pumping since the mechanical pump removed water vapor from the chamber far more rapidly than it could be replenished by evaporation from the dewar.

The first experiments simply recorded the qualitative behavior of the water as the chamber was continuously pumped from 1000 to ~5 mbar. It was seen that, if the surface cooling was

TABLE II
Atmospheric Parameters for Convection and Evaporation Calculation[a]

	Parameter	Typical value	
		Mars[b]	Earth[c]
μ	Dynamic viscosity (kg/m · s)	1.37×10^{-5}	1.72×10^{-5}
k	Conductivity (W/m · K)	0.0145 (soil[d])	0.35 (soil[d])
		2.2 (ice)	2.2 (ice)
c_p	Heat capacity (J/kg · K)	833.8	1005
q_{sc}	Solar constant (W/m^2)	589	1400
g	Gravitational constant (m/s^2)	3.75	9.81
λ_h	Enthalpy of vaporization at 0°C (J/kg)	2.52×10^6	2.52×10^6
ρ	Atmospheric mass density (kg/m^3)	0.020	1.29
ν	Kinematic viscosity (m^2/s)	6.93×10^{-4}	0.133×10^{-4}[e]
α	Thermal diffusivity (m^2/s)	8.83×10^{-4}	0.185×10^{-4}
D	Mechanical diffusivity (m^2/s)	14.0×10^{-4}	0.22×10^{-4}
$\Delta\rho/\rho$	Relative density difference (dimensionless)	0.556	0.0023
ΔC	Concentration difference (g/cm^3)	2.60×10^{-5}	2.60×10^{-5}
e	Saturation vapor pressure of water/ice (mbar)	6.1	6.1
P_0	Atmospheric pressure (mbar)	10	1000
m_w	Molecular weight of water (g/mol)	18	18
m_e	Molecular weight of air (g/mol)	44.0	28.9
Pr	Prandtl number (dimensionless)[f]	0.78 (273 K)	0.72 (273 K)
		0.84 (200 K)	0.74 (200 K)
Re	Reynolds number (dimensionless)[g]	1.44×10^4	75.4×10^4
Gr	Grashof number (dimensionless)[h]	9.2×10^6	3.0×10^{10}
Le	Lewis number (dimensionless)[i]	0.64	0.84
Nu	Nusselt number (dimensionless)[j]	27.9 (free)	418 (free)
		73.4 (forced)	517 (forced)

[a] Note that the quantities μ, k, Pr, and c_p are largely insensitive to pressure. Sources include Holman (1990) and, for diffusion constants, Boynton and Brattain (1929).

[b] For water vapor in dry CO_2 at 10 mbar and 273 K, surrounded by dry air, unless otherwise stated.

[c] For water vapor in air at 1 bar and 273 K, surrounded by dry air, unless otherwise stated.

[d] For dry soil. Conductivity is up to 6 × larger for wet soil on Earth.

[e] Calculated for air at 1 bar, 273 K.

[f] The Prandtl number relates the relative thickness of the hydrodynamic and thermal boundary layers (insensitive to pressure).

[g] The Reynolds number characterizes flow in forced convection. It is calculated here for 10 m/s wind, and 1 m scale length.

[h] The Grashof number is the ratio of buoyancy to viscous forces. It is calculated for 273 K water under 200 K dry CO_2 for Mars, and under 273 K dry air for Earth.

[i] The Lewis number is the ratio of thermal to mechanical diffusivity.

[j] The Nusselt number determines the heat transfer coefficient ($Nu = hL/k$, where L is a characteristic length). Forced convection is calculated for 10 m/s wind.

inadequate, occasional large bubbles were formed, as predicted by theory.[1] With adequate cooling, however, only small dissolved-gas bubbles were observed at all pressures until the surface froze. The dominant effect of reduction of atmospheric pressure is expected to be enhanced evaporative cooling of the surface, eventually leading to freezing. Indeed, crystals of ice were observed to form on the surface at pressures between 6.5 and 13 mbar (5–10 Torr), and these quickly nucleated complete freezing of the surface. Even after tens of minutes of continued pumping, this surface layer seldom grew thicker than a few millimeters. While the ice was reasonably clear, the surface texture was irregular as a result of bubbles that were trapped during the sudden freezing process. (This texture is assumed to be an artifact of sudden pressure reduction and not necessarily typical of martian ice.) Despite the rapid evaporation during the latter stages of this experiment, the pumping rate was adequate to maintain the dewpoint well below 0°C. Since the experiment was performed rapidly, the atmosphere still

[1] Boiling occurs in liquids when bubbles can be nucleated that are large enough for the internal (vapor) pressure to overwhelm the surface tension (e.g., Frenkel 1946). Smaller bubbles collapse; larger bubbles rapidly expand. At Earth's sea-level atmospheric pressure, boiling requires heating to 105–110°C, corresponding to overpressures as large as 1 bar and minimal bubble sizes of micrometer scale. If the external pressure is 4.5 mbar and the internal pressure is the triple point pressure, 6.1 mbar (corresponding to water at 0°C), the minimum bubble size is approximately 1 *milli*meter. If the water temperature significantly exceeds 0°C, the resultant bubbles are extremely large—in this case expanding to the full diameter of the vessel.

consisted predominantly of nitrogen when the liquid froze over.

For the evaporation measurements, the pumps were valved off at the target pressure for intervals of 5–30 min, allowing the evaporation rate to be determined from the rise in the dewpoint. Since the chamber was completely isolated, evaporation from the dewar was the only significant influence on chamber humidity. Actual loss of liquid to evaporation was too small to be detected directly in the vessel but was readily deduced from the rate of dewpoint elevation. Evaporation rates were determined from the dewpoint elevation after the dewpoint is converted to partial pressure of water p_w using empirical equations for the vapor pressure of pure water. Since the buildup of water vapor also suppresses the evaporation rate, the equivalent rate for a dry chamber was calculated from the formula

$$R_{\text{evap}} = \left(\frac{e}{e - p_w}\right) \times \frac{V_{\text{chamber}}\left(\frac{d\rho_w}{dt}\right)}{A_{\text{dewar}}} \qquad (1)$$

where V_{chamber} and A_{dewar} are the volume of the chamber and the surface area of the dewar, respectively, and e is the saturation vapor pressure at the surface temperature.

The results, shown in Fig. 3, confirm that the power-law behavior predicted by the theoretical model is at least qualitatively correct over the entire pressure range, particularly since variations of a factor of 2 are not of significance compared to variations in the natural environment that is being modeled. Some of the experimental variation is an artifact of the hygrometer calibration, which sometimes drifted as much as 2°C in the course of a measurement. Accordingly, the error bars in Fig. 3 reflect a possible error of ±2° in dewpoint, added in quadrature to the small standard deviation of the fit to each time–dewpoint series. For reference, the point marked with an "X" represents an empirical model of evaporation on Earth at 0°C (cited in Holman 1990, p. 612).

Systematic variations in evaporation rate between runs were greater than the variation within a single run, although each run showed the expected pressure dependence. The most likely source of this variation was a difference in the actual surface temperature of the liquid, which was exposed to both room-temperature air and bright illumination from above. While this temperature was not measured during the experiment, the results do seem consistent with the method of cooling, which varied slightly from run to run. In the first run (data set #1), ice cubes were held in place at the base of the dewar by a coarse screen. This method was replaced in the second run (data set #2) by a block of ice frozen into the base of the dewar. Bubbling at low pressure indicated that this was the least satisfactory approach, presumably because of the relatively small contact

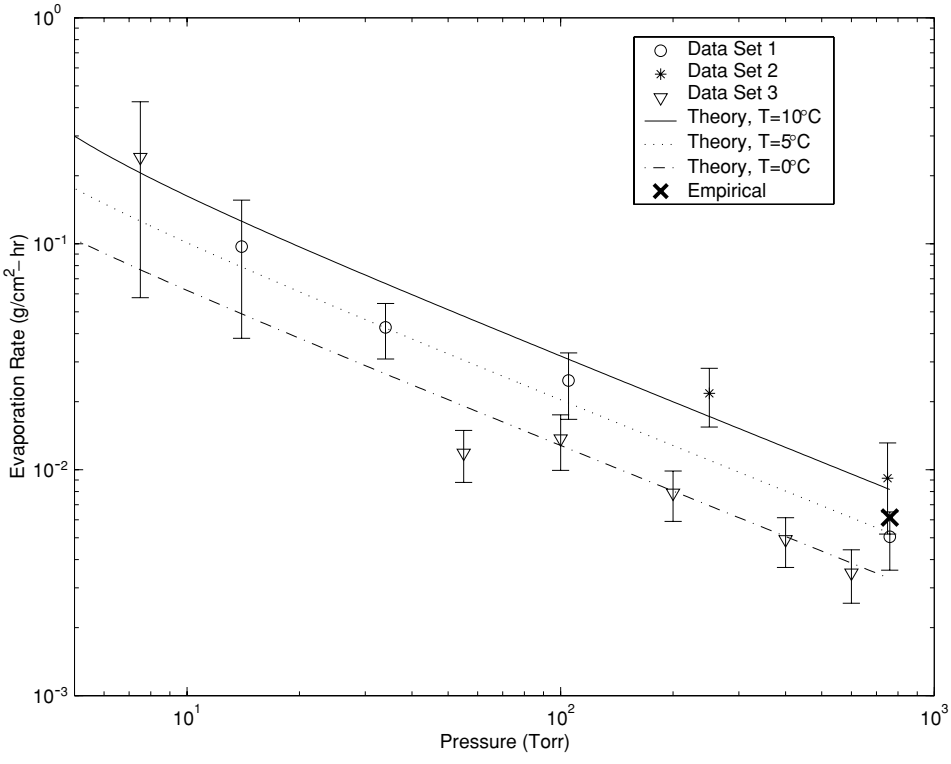

FIG. 3. Measured evaporation rates compared to theoretical model, assuming various surface temperatures (see text). Each run used a different cooling method. Theoretical fits are qualitatively consistent with the suspected surface temperatures. The empirical model is for Earth conditions.

area between the ice and the liquid. In the final run (data set #3), the ice cubes were formed around small lead weights to make them denser than the surrounding water. This technique allowed the greatest ratio of ice to water and appeared to provide the most effective cooling. This qualitative assessment of surface temperature is consistent with calculations of the evaporation rate at 0, 5, and 10°C, using the model proposed by Ingersoll (1970). In particular, data set #3 is well described by the calculation for 0°C, shown by the dot-dash line.

While evaporation from a small vessel in a still, closed container may be a poor representation of an open landscape on Mars, the general agreement among theory, experiment, and empirical measurements on Earth provide encouragement for this approach.

INSOLATION

Insolation will be at a maximum when the solar angle is normal to the local slope. In practice, this limits both the slope and the orientation of gullies. At latitudes L poleward of 25°, the minimum equator-facing slope that satisfies this condition is $s > L - I$, where the present-day inclination $I = 25°$. Poleward of 65°, pole-facing slopes can satisfy this condition in midsummer if $s > I + L - 90$.

The approximate formula for the maximum insolation at normal incidence illumination is

$$I_{\text{sol}} = (1 - R))I_0 e^{(-\tau/\cos\theta)}, \tag{2}$$

where I_0 is the solar constant (589 W/m^2 average), R is the albedo, τ is the optical depth (typically varying from 0.1 to 1.0, with lower values common at higher altitudes), and θ is the slope angle. On Mars, the albedo ranges from 0.1 to 0.35, with low values characteristic of the subpolar latitudes where gullies are prevalent (Mellon *et al*. 2000). In addition, the gullies typically appear dark in an optical image, indicating a low albedo.

For these calculations, the solar constant was adjusted for the eccentricity of Mars' orbit, favoring the southern summer solstice which occurs near perihelion. Diffuse scattering was added, following Pollack 1990. Reflected light from nearby surfaces, which could enhance the total insolation on slopes (Mellon and Phillips 2001), was *not* considered. Figure 4 illustrates the incident radiation on a sun-facing slope as a function of zenith angle, which can be quite high for a pole-facing slope, even in midsummer. In that respect, higher latitudes are favored for melting, since the summer sun rises higher in the sky over the pole.

Since for dry soil the radiation/insolation balance primarily determines the surface temperature, Fig. 4 also indicates that

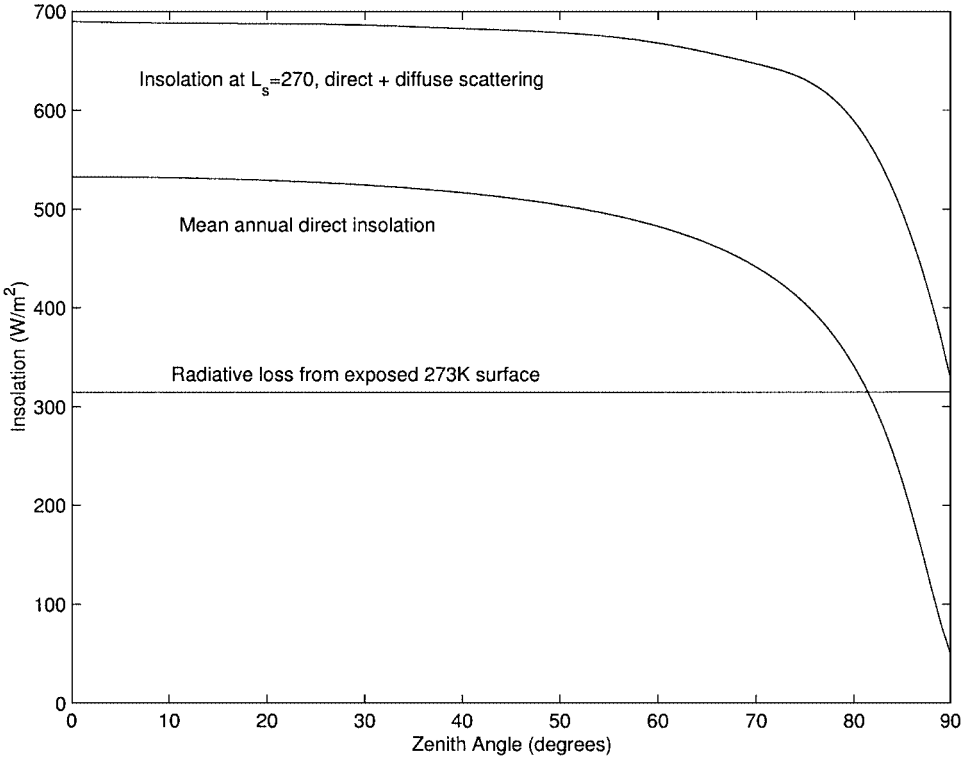

FIG. 4. Maximum insolation as a function of zenith angle for a Sun-facing slope, assuming an optical depth of 0.1, zero albedo, and a scale height of 11 km. The bottom curve shows the mean annual value; the top is for southern summer solstice, near perihelion and includes diffuse scattering. Typical radiative loss from the surface of exposed water/ice is shown for comparison.

peak temperatures exceeding 0°C may be obtained even at high latitudes.

RADIATION

Radiative cooling to the cold martian sky is a dominant factor in determining thermal balance. The radiative loss is typically written

$$I_{\text{rad}} = \varepsilon a\left(T^4 - T_{\text{sky}}^4\right), \tag{3}$$

where ε is the emissivity, assumed to be at least 0.95 (typical of most minerals), and the Stefan–Boltzmann constant $a = 5.7 \times 10^{-8}$ W/m$^2 \cdot$K^4. The martian sky is assumed to be extremely cold and to contribute a negligible amount of heat to the surface of melting ice. Earth's sky, by comparison, is often as warm as 260 K, barely colder than the melting point of ice. As a result, radiative losses to the sky are at least six times greater on Mars than on Earth. Radiation alone (at the melting point of water) may equal or exceed insolation on Mars. Significantly, however, when the Sun is at normal incidence to a local surface and when the sky is clear, the radiative equilibrium temperature may still equal or exceed 273 K anywhere on the planet.

Even allowing for efficient collection of sunlight, melting of ice would still be overwhelmed by the combination of radiative and evaporative cooling. In practice, however, radiative losses may be markedly less than implied by Eq. (3). Radiative heat loss always reflects a balance between radiation of the object and radiation received from the sky and other line-of-sight surfaces. Equation (3) assumes that an icy surface radiates into 2π solid angle of sky, an assumption valid only for flat surfaces. In shallow basins, in gullies, or below scarps, radiation from melting surfaces to the sky may be sharply reduced. In essence, these geometries provide "shade" from the cold sky, in much the same way that a dewshield keeps a telescope mirror warm. This factor can be incorporated into Eq. (3) by replacing ε with an apparent emissivity, $\varepsilon_{\text{app}} = \varepsilon\Omega'/2\pi$, which is scaled by the fraction of the sky actually visible from the object. This substitution assumes that other line-of-sight surfaces are in radiative balance with the object, which in practice means that they are at the same temperature.

Among the structures that would be geometrically shielded from radiation are gullies that might carry water or the alcoves where gullies are seen to originate. Lacking constant sunlight, these sheltered locations will usually be cold. When exposed to the Sun, however, they can be warmer than their surroundings. The same phenomenon is implicit in the results of Kossacki *et al.* (2000, 2001), which suggest high peak temperatures inside a robotically excavated trench, and was invoked by Svitek and Murray (1990) to explain redistribution of frost around the Viking lander. In practice, there is an optimal aspect ratio that encourages melting or sublimation. Too deep, and the Sun will shine on the bottom too infrequently. Too shallow, and the radiative losses to the sky prohibit effective heating. Sun-cups in ice and snow might, therefore, be expected to follow surfaces of constant, optimal ε_{app}.

Consider a shallow basin with walls at comparable temperature to an icy surface in the floor. By approximating the basin as a cylindrical hole with radius R, the fractional solid angle $(\Omega'/2\pi)$ of exposed sky can be calculated as

$$\Omega'/2\pi = 1 - \frac{1}{\pi}\int_0^{\pi} \frac{d\varphi}{\sqrt{\tan^2\theta + 1}}, \tag{4}$$

where

$$\tan\theta = \frac{\left(\sqrt{r^2\cos^2\varphi + (1 - r^2)} + r\cos\varphi\right)}{z}$$

and the dimensionless depth z and radius r are measured in units of the total radius R. At the center of the hole, this reduces to $\Omega'/2\pi = 1 - z(z^2 + r^2)^{-1/2}$.

Using this fractional solid angle to determine the apparent emissivity, Fig. 5 maps the apparent emissivity across the bottom of the hole for height-to-diameter ratios between 0 (flat surface) and 2. For example, a point on the bottom of a pit with 45° walls, corresponding to a 1 : 2 height : diameter ratio, radiates less than 30% as much as a free surface, but can still receive 6 hours of sunlight per sol. A dramatic reduction in radiative losses can be seen for even the shallowest basin, particularly at the edges. The apparent emissivity ε_{app}, can readily be a factor of 2 or more smaller than the overall emissivity, ε. This effect can be dramatically observed in recent MGS photos of frost in craters (Fig. 6). The absence of frost near the walls corresponds to regions suffering the least radiative cooling.

EVAPORATIVE AND CONVECTIVE COOLING

The total rate of gas evolution from the surface of liquid water or ice can be determined from the known vapor pressure (Hardy 1998). But as long as the vapor pressure exceeds the total ambient atmospheric pressure, the evaporation rate is limited by the diffusion of this vapor from the humid boundary layer into the dry atmosphere. (If the atmospheric pressure is too low, as over much of the southern highlands, the evaporation rate can be calculated from the Bernoulli equation, $m'/A = \rho v_0 \approx (2\rho\Delta p)^{1/2}$, assuming $\rho v_0^2/2 \approx \Delta p$, where Δp is the overpressure and v_0 is the velocity normal to the surface. This unstable condition causes rapid cooling and, if necessary, freezing of the surface until a stable temperature is restored and evaporation is again diffusion-limited.)

Convection and evaporation are closely related because both depend on the motion of low-density air away from the boundary layer above the water. This motion is seldom due to diffusion alone but is typically aided by wind (forced convection/evaporation) or buoyancy (free convection/evaporation). In the latter case, buoyancy of the air in the boundary layer is due to its higher temperature or lower density (since water vapor is less dense than either martian or terrestrial air).

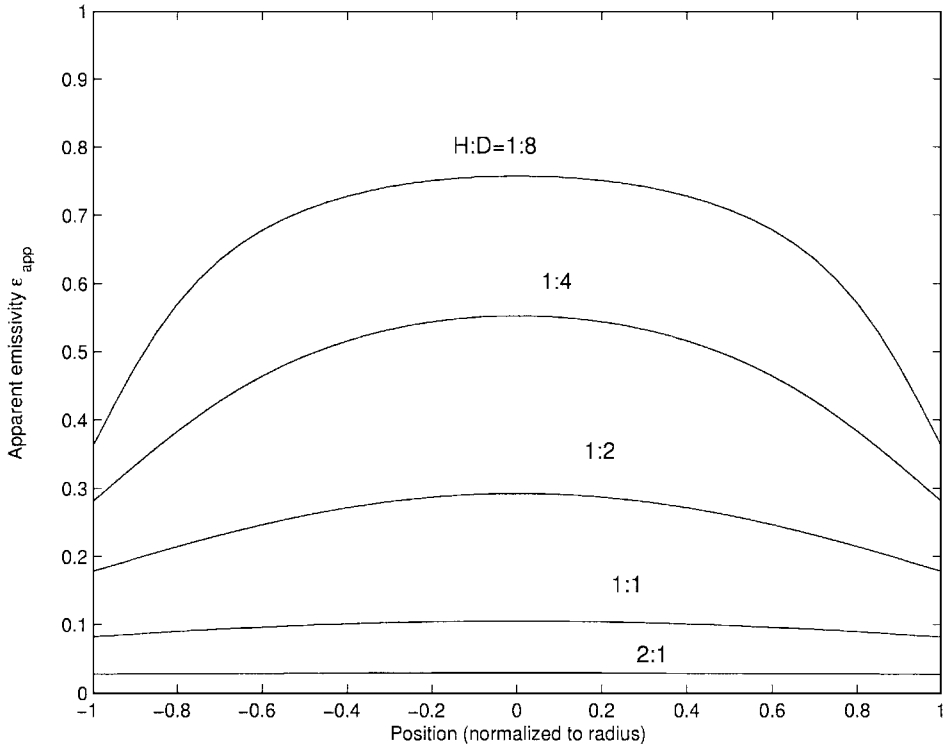

FIG. 5. Apparent emissivity across the floor of a basin, for various depth to diameter ratios. $H/D = 0$ corresponds to a flat surface.

The following derivation of evaporation and convection rates parallels the presentation by Holman (1990), but can be found in most texts on heat transfer (e.g., Jakob 1949, Frenkel 1946). Nomenclature is summarized in Table II.

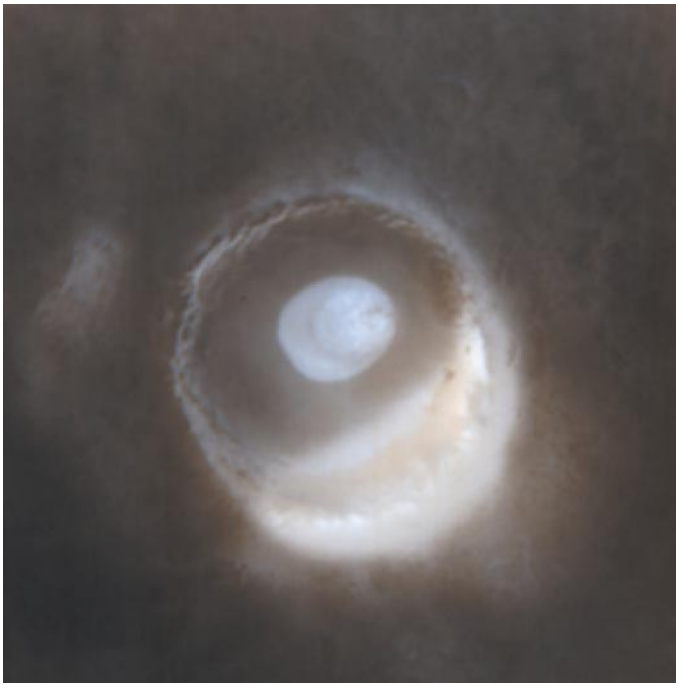

FIG. 6. MOC2-258b, northern spring, 71°N, 257°W, Unnamed Crater, October 6, 2000; crater is 48 km (30 miles) across. (Malin 2000).

In general, the rate of heat transfer q per unit area A from a warm wall at temperature T_{wall} to a cold atmosphere at temperature T_∞ can be written in terms of a heat transfer coefficient h as

$$\frac{q}{A} = h(T_{\text{wall}} - T_\infty). \tag{5}$$

The dimensionless Nusselt number is proportional to the heat transfer coefficient and can be written

$$Nu = \frac{hx}{k}, \tag{6}$$

where k is conductivity, and the convective heat loss is determined by the equation

$$q = h\Delta T = Nu\left(\frac{k\Delta T}{x}\right). \tag{7}$$

Depending on conditions and geometry, the Nusselt number is typically a function of the Prandtl number and either the Grashof number (free convection) or the Reynolds number (forced convection). The Prandtl number, $Pr = c_p\mu/k$, relating the relative thickness of the hydrodynamic and thermal boundary layers, has a value near unity. It is relatively insensitive to pressure and its value is not significantly different on Earth from that on Mars. In contrast, the Reynolds number, which describes forced convection, is markedly smaller on Mars than on Earth. This implies that convective flow is more laminar and less turbulent on Mars than under similar terrestrial conditions.

The dependence of convection and evaporation on properties such as atmospheric pressure, temperature, gravity, or gas composition (the properties that distinguish Earth from Mars in this respect) is captured in the dimensionless Grashof number, the ratio of buoyancy to viscous forces. The Grashof number is generally written

$$Gr = \frac{\rho^2 g \beta \Delta T x^3}{\mu^2}, \tag{8}$$

where the volume coefficient of expansion

$$\beta = \frac{1}{V}\left(\frac{\partial V}{\partial T}\right)_p = \begin{cases} \frac{1}{\rho}\frac{\Delta\rho}{\Delta T} & \text{for mass convection (evaporation),} \\ \frac{1}{T} & \text{for thermal convection,} \end{cases}$$

μ is the dynamic viscosity (evaluated at ∞), ρ is the total density of saturated gas at the evaporating surface, x is a characteristic dimension (x will cancel for free convection), g is gravitational acceleration, V is a volume element, T is the gas temperature, and Ingersoll (1970) suggests

$$\frac{\Delta\rho}{\rho} = \frac{(\rho_\infty - \rho)}{\rho} = \frac{(m_e - m_w)e}{m_e P_0 - (m_e - m_w)e},$$

where e = saturation vapor pressure of the evaporating water (or ice), P_0 = total atmospheric pressure, m_w = molecular weight of water, and m_e = molecular weight of air.

For evaporation (mass convection), the Grashof number can be rewritten as

$$Gr = x^3\left[\frac{g\left(\frac{\Delta\rho}{\rho}\right)}{v^2}\right], \tag{9}$$

where $v = \mu/\rho$ = kinematic viscosity (evaluated at ∞).

Free convection assumes that gravity (buoyancy) is the driving force. It is derived assuming a vertical wall; the results are then empirically extended to horizontal surfaces. Forced convection, derived assuming a *horizontal* wall, assumes that sheer stress from wind is the driving source. An estimate of the relative contribution of free and forced convection can be determined from the relevant force gradients, ρg for free convection and $\rho v^2/L$ for forced convection. Thus, for example, if the length scale were $L = 1$ m at Mars atmospheric pressure, the crossing point between free and forced convection would be 1–2 m/s.

Assuming free convection as in Fig. 2 (appropriate for wind speeds below ~2 m/s), the Nusselt number can be determined from the Grashof and Prandtl numbers,

$$Nu_f = 0.15(Gr_f Pr_f)^{1/3} = \frac{hx}{k}, \tag{10}$$

where the subscript f indicates that the quantities are evaluated at the film temperature, T_f, the average of air and wall temperatures $(T_\infty + T_{\text{wall}})/2$. The scale factor 0.15 and the exponent 1/3 are applicable for Rayleigh numbers ($Ra = GrPr$) between 8×10^6 and 1×10^{11}, more or less the range spanned by conditions on Earth and Mars. Note that the heat transfer coefficient h is not dependent on x in this special case.

By comparison, for forced convection (as in Fig. 1),

$$Nu_f = 0.664 Re_f^{1/2} Pr_f^{1/3}. \tag{11}$$

Equations analogous to thermal convection describe the rate of mass transfer m' in terms of a difference in concentration ΔC (mass/volume solute) and a mass transfer coefficient h_D:

$$m'/A = h_D(C_{\text{surf}} - C_\infty). \tag{12}$$

Since heat and mass transfer coefficients both reflect movement of air and diffusion of molecules in response to the same forces and both vary with ambient gas pressure, but in an opposing sense, mass convection is favored in thin air because the mean free path lengthens and heat convection is favored in dense air as more molecules participate in the heat exchange process. It can be shown (again, see Holman 1990) that the ratio of the transfer coefficients, and hence the ratio of convective to evaporative cooling, is

$$h/h_D = \rho c_p Le^{2/3}, \tag{13}$$

where ρ is the mass density, c_p is the heat capacity, and the Lewis number $Le = \alpha/D$, the value of which is close to unity, reflects the subtle difference between thermal diffusivity, $\alpha = k/\rho c_p$, and mechanical diffusivity, D.

Thus, in this formalism, the evaporative mass loss is[2]

$$E = h_d \Delta C = 0.15 \times (D\Delta C/x)(Gr_f Pr_f Le)^{1/3}, \tag{14}$$

where ΔC is the difference in vapor concentration (mass/volume solute) between the surface and the surrounding atmosphere, and ρ_w is the density of water vapor at the source temperature and vapor pressure.

Using this formalism, the evaporation formula of Ingersoll (1970) can be written as a simplified version of Eq. (14):

$$E = (0.17)D\Delta C\left[\frac{g\left(\frac{\Delta\rho}{\rho}\right)}{v^2}\right]^{1/3} = (0.17)\frac{D\Delta C}{x}Gr^{1/3}. \tag{15}$$

Figure 7 compares both forms for Earth and Mars gravity and gas composition.

Following Eq. (13), Fig. 8 compares evaporative and convective cooling from a body of liquid water (possibly ice encrusted) under a cold, 200 K atmosphere. It can be seen that the total heat

[2] For evaporation, the equivalent of the Nusselt number is conventionally called the Sherwood number *Sh*. The analogy to Eq. (11) is $Sh_f = 0.15 \times (GrSc)^{1/3} = h_d x/D$, where, to emphasize the analogy, the Prandtl number has been replaced by the Schmidt number, $Sc = v/D = (\alpha/D)Pr = LePr$. Note that the Lewis number is near unity.

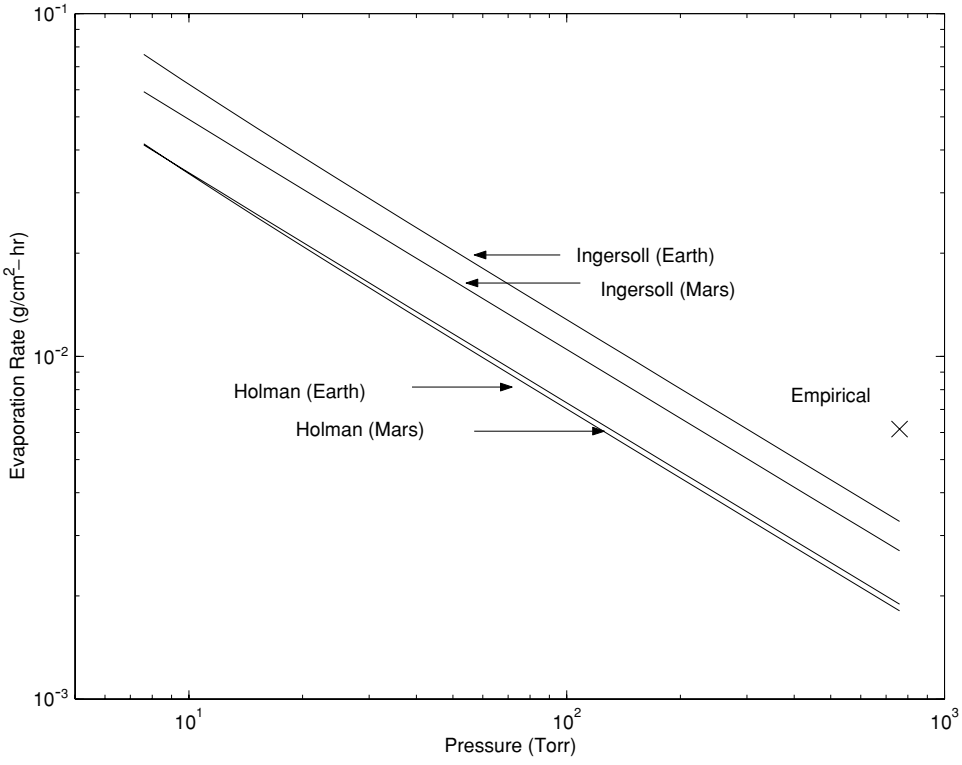

FIG. 7. Using either the model of Eq. (15) ("Ingersoll") or Eq. (14) ("Holman"), predicted evaporation rates as a function of pressure on Mars (in CO_2) and on Earth (in air or N_2) are nearly identical. All calculations are for 0°C. An empirical value for terrestrial evaporation is shown for comparison.

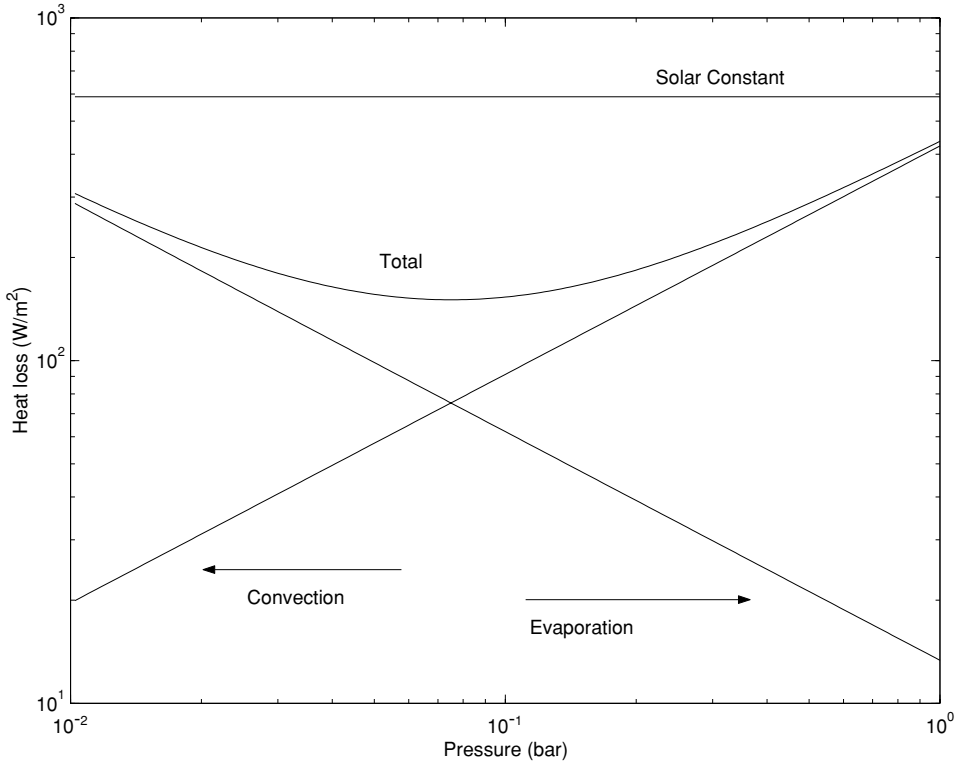

FIG. 8. Convective heat transfer between a 273 K surface (water) and a 200 K atmosphere compared to evaporative cooling. The right-hand boundary reflects terrestrial conditions; the left reflects martian conditions. For equivalent conditions, total heat loss is actually less on Mars than on Earth.

loss due to the two mechanisms is actually *less*, for equivalent temperatures, on Mars than on Earth. Minimal heat loss would occur when the two loss mechanisms were comparable, at approximately 80 mbar. Convective cooling on Mars is equivalent to that produced by only a few degrees of temperature difference (ΔT) on Earth. By contrast, the evaporative cooling of this water on Mars is substantially greater than on Earth.

Evaporation may be suppressed when the equilibrium surface temperature falls below 0°C, thereby lowering the vapor pressure at that surface. That temperature may be lowered by an insulating ice barrier between the ice–water interface and the water–air interface or by an actual reduction in melting point due to salinity. For example, since the cryoscopic constant for water is $K_f = 1.86$ K · kg/mol at 0°C, 3 mol/liter of a solute lowers the melting point to −5.58°C, lowering the vapor pressure to 3.8 mbar from 6.1 mbar. (For comparison, the salinity of seawater is less than 0.7 mol/liter, while that of the Dead Sea is nearly 6 mol/liter). Included in this calculation is a small (5%) suppression of evaporation directly associated with the solvent, following Raoult's law.

Coatings of dust (Farmer 1976) or other contaminants can also suppress evaporation. In addition, the buoyancy-based free convection calculation is not necessarily the most generous assumption. Haberle *et al*. (2001) suggest that such a calculation may overstate the actual evaporation rate by as much as a factor of 4.

CONDUCTION

The dry martian soil is highly insulating. Ice, by comparison, is highly conducting. Thus the areas most conducive to melting are those in which thin ice overlays dry soil. The conductive loss to soil will vary with time as the streambed warms up. The one-dimensional solution to the time-dependent heat-loss equation is

$$q(t) = k(T_{\text{surf}} - T_{\text{soil}})/\sqrt{\pi \alpha t}, \tag{16}$$

where $\alpha = k/\rho C_p$, ρ is the soil density, k is the conductivity, and C_p is the heat capacity.

Ice ($\rho = 0.9$ g/cm^3) is relatively conducting, with $k = 0.022$ W/cm · K and $C_p = 2.01$ J/g · K. Soil ($\rho = 1.5$ g/cm^3), however, may be highly insulating, with some authors (e.g., Kieffer and Zent 1992) suggesting values as low as $k = 0.00077$ W/cm · K and $C_p = 0.59$ J/g · K. These two cases are illustrated in Fig. 9.

DISCUSSION

Over most of the land mass of Earth the relative humidity is less than 100% (or the temperature is below 0°C), and liquid water is out of equilibrium with the atmosphere. Despite this disequilibrium, water on Earth is metastable with

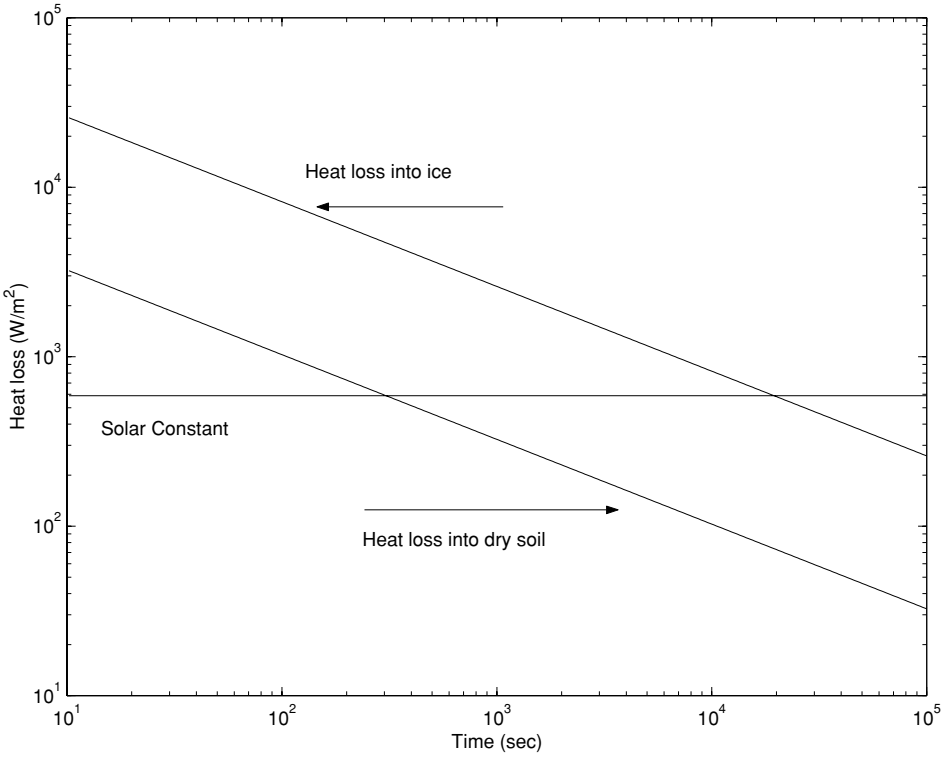

FIG. 9. Heat loss as a function of time from 273 K water into a 200 K streambed. The Mars solar constant is shown for reference. It requires at least an hour for the dry soil to warm sufficiently to allow melting; several hours are required for ice.

respect to evaporation or freezing on a scale of hours, days, or years. On Mars, liquid water is similarly metastable, primarily with respect to freezing, and evaporative cooling, rather than convection, is the engine of freezing. Evaporation at 0°C on Mars is comparable to evaporation at 60°C on Earth, and freezing, at similar temperatures, is comparable on the two planets.

Even under contemporary conditions, the flow of small quantities of liquid water over short distances may result from ice-melt on Mars. Poor atmospheric convection and low soil conductivity allow for local warm patches nearly anywhere on the planet. Under the favorable circumstances described here (shallow basins, sun-facing slopes, clear skies, reduced surface temperature, and ice overlying soil), the thermal balance in Fig. 2 indicates that in excess of 100 W/m^2 net heat input may be available to melt ice. It has been shown elsewhere (e.g., Carr 1983, McKay and Davis 1991) that liquid water can readily flow for many hours on Mars without significant refreezing. Even more extreme conditions, such as lowered evaporation rates due to surficial diffusion barriers, could enhance the rate of melt.

If the gullies are, indeed, regularly resurfaced by meltwater, then their cold, sheltered locations suggest that the mechanism is source-limited. It is suggested here that such melting could result from winter condensation, which is redistributed and concentrated in early spring and then melted when sunlight first shines directly into the gully. This mechanism is similar to that observed by Lee *et al*. (2001), who reported late-season runoff from accumulation of ice in alcoves in terrestrial arctic terrain. On Mars, the heating must be sudden for the ice to melt before it sublimates, a condition satisfied by locations in perpetual winter darkness (currently poleward of ±65° latitude). The result could be a shallow, ice-crusted stream, or a melting–freezing cycle that promotes erosion through mechanical fracture.

The source of the hypothesized seasonal ice could be cold-trapping of a winter frost layer, as invoked by Svitek and Murray (1990) to explain the winter frost redistribution at the Viking 2 site. They concluded that a uniform 10–20 μm thick frost layer was converted to frost patches, 100–200 μm thick, covering the most sheltered 10% of the surface. Thermal analysis indicates that the process is driven by warming of the surface, which sublimes the frost into the cold, already-saturated atmosphere and is limited only by the supply of vapor. Equilibrium is established by condensation onto shaded areas.

At the higher latitudes of the gullies, a substantially thicker uniform frost layer would be expected, in part because the column abundance of water is greater (Jakosky and Haberle 1992) and in part because of the extended winter period without insolation. The higher contrast of the gully region topography compared to the Viking Lander 2 site should significantly increase the concentration ratio, as abrupt depressions on the sides of slopes are more efficient at collecting wind-blown ice fog than the rock-sheltered traps at the Viking site. While a detailed analysis is beyond the scope of this discussion, it does not seem unreasonable that millimeters to centimeters of water ice could accumulate seasonally by this mechanism. It is an open question whether such small quantities of water are sufficient to form gullies or simply to continuously resurface and preserve gullies formed by transient events.

SUMMARY

Three factors constrain the melting of ice on Mars. First, the radiative balance must be optimized by a clear, sunny, windless day; a low albedo surface; a slope that faces the Sun for part of the day; and a geometry that shields the surface from part of the sky. Second, conductivity to the bed must be small, a condition met by martian soil but not by thick ice. Third, the surface temperature must be suppressed a few degrees, perhaps by formation of an ice crust or by incorporation of salts in the water. In addition, the factor that probably determines the *location* of runoff features is the accumulation of ice itself. It is suggested that this accumulation may simply result from a concentration of winter frost from surrounding areas.

ACKNOWLEDGMENTS

I am grateful to Tom Pike, Tom Meloy, Martin Frant, Frank Grunthaner, Aaron Zent, Chris McKay, and Jules Goldspiel for useful discussion in preparation of this manuscript. The work presented here was carried out at the Jet Propulsion Laboratory, California Institute of Technology, under contract to the National Aeronautics and Space Administration (NASA). Funding was provided by NASA's Office of Life and Microgravity Sciences and Applications (OLMSA), as part of the support for the Mars Environmental Compatibility Assessment (MECA) payload developed for the Mars 2001 Surveyor Lander.

REFERENCES

Berry, R. S., S. A. Rice, and J. Ross 1980. *Physical Chemistry*. Wiley, New York.

Boynton, W. P., and W. H. Brattain 1929. Diffusion in gases. In *International Critical Tables* (E. M. Washburn, Ed.), Vol. 5, p. 63. McGraw-Hill, New York.

Carr, M. H. 1983. Stability of streams and lakes on Mars. *Icarus* **56**, 476–495.

Clow, G. D. 1987. Generation of liquid water on Mars through the melting of a dusty snowpack. *Icarus* **72**, 95–127.

Farmer, C. B. 1976. Liquid water on Mars. *Icarus* **28**, 279–289.

Frenkel, J. 1946. *Kinetic Theory of Liquids*. Clarendon, Oxford.

Goldspiel, J. M., and S. W. Squyres 2000. Groundwater sapping and valley formation on Mars. *Icarus* **148**, 176–192.

Haberle, R. M., M. M. Joshi, J. R. Murphy, J. R. Barnes, J. T. Schofield, G. Wilson, M. Lopez-Valverde, J. L. Hollingsworth, A. F. C. Bridger, and J. Schaeffer 1999. General circulation model simulations of the Mars Pathfinder atmospheric structure investigation/meteorology data. *J. Geophys. Res.* **104**, 8957–8974.

Haberle, R. M., C. P. McKay, J. Schaeffer, N. A. Cabrol, E. A. Grin, A. P. Zent, and R. Quinn 2001. On the possibility of liquid water on present-day Mars. *J. Geophys. Res.* **106**, 23,317–23,326.

Hardy, B. 1998. ITS-90 Formulations for vapor pressure, frostpoint temperature, dewpoint temperature, and enhancement factors in the range −100 to +100 C. In *Proc. Third International Symposium on Humidity & Moisture*, Teddington, London, England, April 1998. Online at http://www.thunderscientific.com/reflibrary/its90formulas.pdf.

Holman, J. P. 1990. *Heat Transfer,* 7th ed., McGraw-Hill, San Francisco.

Ingersoll, A. P. 1970. Mars: Occurrence of liquid water. *Science* **168**, 972–973.

Jakob, M. 1949. *Heat Transfer.* Wiley, New York.

Jakosky, B. M., and R. M. Haberle 1992. The seasonal behavior of water on Mars. In *Mars* (H. H. Kieffer, B. M. Jakosky, C. W. Snyder, and M. S. Matthews, Eds.), pp. 969–1016. Univ. of Arizona Press, Tucson.

Kahn, R. 1985. The Evolution of CO_2 on Mars. *Icarus* **62**, 175–190.

Kahn, R. 1990. Ice haze, snow, and the Mars water cycle. *J. Geophys. Res.* **95**, 14667–14693.

Kieffer, H. H., and A. P. Zent 1992. Quasi-periodic climate change on Mars. In *Mars* (H. H. Kieffer, B. M. Jakosky, C. W. Snyder, and M. S. Matthews, Eds.), pp. 1180–1218. Univ. of Arizona Press, Tucson.

Kossacki, K. J., W. J. Markiewicz, and H. U. Keller 2000. Small scale trench in the martian soil: Conditions for condensation of atmospheric volatiles. *Icarus* **144**, 463–478.

Kossacki, K. J., W. J. Markiewicz, and H. U. Keller 2001. Effect of surface roughness on ice distribution in the south subpolar region of Mars. *Planet. Space Sci.* **49**, 437–445.

Lee, P., C. S. Cockell, M. M. Marinova, C. P. McKay, and J. W. Rice Jr. 2001. Snow and ice melt flow features on Devon Island, Nunavut, Arctic Canada as possible analogs for recent slope flow features on Mars. *Lunar Planet. Sci.* **32**, 1809 (abstract). [CD-ROM]

Leovy, C. 2001. Weather and climate on Mars. *Nature* **412**, 245–294.

Malin, M. C., and K. S. Edgett 2000. Evidence for recent groundwater seepage and surface runoff on Mars. *Science* **288**, 2330.

Malin, M. C., K. S. Edgett, M. H. Carr, G. E. Danielson, M. E. Davies, W. K. Hartmann, A. P. Ingersoll, P. B. James, H. Masursky, A. S. McEwen, L. A. Soderblom, P. Thomas, J. Veverka, M. A. Caplinger, M. A. Ravine, T. A. Soulanille, and J. L. Warren 2000. Unnamed Crater. *NASA's Planetary Photojournal*, MOC2-258b, created November 27, 2000. Available at http://photojournal.jpl.nasa.gov.

McKay, C. P., and W. L. Davis 1991. Duration of liquid water habitats on early Mars. *Icarus* **90**, 214–221.

Mellon, M. T., and R. J. Phillips 2001. Recent gullies on Mars and the source of liquid water. *J. Geophys. Res.* **106**, 23,165–23,180.

Mellon, M. T., B. M. Jakosky, H. H. Kieffer, and P. R. Christensen 2000. High-resolution thermal inertia mapping from the Mars Global Surveyor thermal emission spectrometer. *Icarus* **148**, 437–455.

Pollack, J. B., R. M. Haberle, J. Schaffer, and H. Lee 1990. Simulations of the general circulation of the martian atmosphere. *J. Geophys. Res.* **95**, 1447–1473. [These results are used as described in Rapp, D., S. Dawson, G. Wilson, D. Crisp, N. Mardesich 2001. Solar Power on Mars. Unpublished JPL document.

Smith, M. D., J. C. Pearl, B. J. Conrath, and P. R. Christensen 2001. Thermal emission spectrometer results: Mars atmospheric thermal structure and aerosol distribution. *J. Geophys. Res.* **106**, 23,929–23,945.

Svitek, T., and B. Murray 1990. Winter frost at Viking Lander 2 site. *J. Geophys. Res.* **95**, 1495–1510.

Wallace, D., and C. Sagan 1979. Evaporation of ice in planetary atmospheres: Ice-covered rivers on Mars. *Icarus* **39**, 385–400.

Wolff, M. J., J. F. Bell III, P. B. James, R. T. Clancy, and S. W. Lee 1999. Hubble Space Telescope observations of the martian aphelion cloud belt prior to the Pathfinder mission: Seasonal and interannual variations. *J. Geophys. Res.* **104**, 9027–9041.

Zurek, R. 1992. Comparative aspects of the climate of Mars: An introduction to the current atmosphere. In *Mars* (H. H. Kieffer, B. M. Jakosky, C. W. Snyder, and M. S. Matthews, Eds.), pp. 835–933. Univ. of Arizona Press, Tucson.